Human Molecular Genetics, 2010, Vol. 19, No. 4 **634–647**
doi:10.1093/hmg/ddp531
Advance Access published on December 16, 2009

Specific saposin C deficiency: CNS impairment and acid β-glucosidase effects in the mouse

Ying Sun[1,4], Huimin Ran[1,4], Matt Zamzow[1,4], Kazuyuki Kitatani[6], Matthew R. Skelton[2,4], Michael T. Williams[2,4], Charles V. Vorhees[2,4], David P. Witte[3,5], Yusuf A. Hannun[6] and Gregory A. Grabowski[1,4,*]

[1]The Division of Human Genetics, [2]Division of Neurology and [3]Division of Pediatric Pathology, Cincinnati Children's Hospital Medical Center, Cincinnati, OH, USA, [4]Department of Pediatrics and [5]Department of Pathology, University of Cincinnati College of Medicine, Cincinnati, OH 45229-3039, USA and [6]Department of Biochemistry and Molecular Biology, Medical University of South Carolina, Charleston, SC 29425, USA

Received July 15, 2009; Revised October 13, 2009; Accepted November 24, 2009

Saposins A, B, C and D are derived from a common precursor, prosaposin (*psap*). The few patients with saposin C deficiency develop a Gaucher disease-like central nervous system (CNS) phenotype attributed to diminished glucosylceramide (GC) cleavage activity by acid β-glucosidase (GCase). The *in vivo* effects of saposin C were examined by creating mice with selective absence of saposin C (C−/−) using a knock-in point mutation (cysteine-to-proline) in exon 11 of the *psap* gene. In C−/− mice, prosaposin and saposins A, B and D proteins were present at near wild-type levels, but the saposin C protein was absent. By 1 year, the C−/− mice exhibited weakness of the hind limbs and progressive ataxia. Decreased neuromotor activity and impaired hippocampal long-term potentiation were evident. Foamy storage cells were observed in dorsal root ganglion and there was progressive loss of cerebellar Purkinje cells and atrophy of cerebellar granule cells. Ultrastructural analyses revealed inclusions in axonal processes in the spinal cord, sciatic nerve and brain, but no excess of multivesicular bodies. Activated microglial cells and astrocytes were present in thalamus, brain stem, cerebellum and spinal cord, indicating regional pro-inflammatory responses. No storage cells were found in visceral organs of these mice. The absence of saposin C led to moderate increases in GC and lactosylceramide (LacCer) and their deacylated analogues. These results support the view that saposin C has multiple roles in glycosphingolipid (GSL) catabolism as well as a prominent function in CNS and axonal integrity independent of its role as an optimizer/stabilizer of GCase.

INTRODUCTION

Saposin C is one of four saposins (A, B, C and D) that derive from a common precursor, prosaposin, by proteolytic processing in the late endosome (1). Each saposin is an 80 amino acid lysosomal glycoprotein with a role in enhancing the activity of specific cognate enzymes in GSL degradation (2). Saposin B presents a specific GSL, sulfatide, to its hydrolase, arylsulfatase A, for cleavage to galactosylceramide (3). In both humans and mice, saposin B deficiency results in sulfatide accumulation and a metachromatic leukodystrophy-like disease that is similar to arylsulfatase A deficiency (4,5). Saposin C interacts with GCase, leading to optimal activity (6). Biochemical studies have shown that in addition to its activation function toward GCase, saposin C protects GCase from proteolytic degradation (7). Point mutations in saposin C lead to a Gaucher-like disease due to diminished GC cleaving activity in cells (8,9). Both saposin B and C have *in vitro* effects on hydrolysis of LacCer by activation of galactosylceramide-β-galactosidase, GM1-β-galactosidase and other β-galactosidases (10). *In vitro*, saposins A and C enhance GCase activity in the presence of negatively charged phospholipids, but saposin A and C have

*To whom correspondence should be addressed at: Division of Human Genetics, Cincinnati Children's Hospital Research Foundation, 3333 Burnet Avenue, Cincinnati, OH 45229-3039, USA. Tel: +1 5136367290; Fax: +1 5136362261; Email: greg.grabowski@cchmc.org

different membrane interaction modes (11,12). *In vivo*, saposin A and C specifically enhance the activities of galactosylcerebrosidase and GCase, respectively (13). Saposin D facilitates acid ceramidase degradation of ceramide to sphingosine and fatty acids (14).

The structure of saposin C is restrained by three disulfide bonds (15). Biophysical studies have shown that saposin C has membrane fusion properties (16,17). This fusion occurs by the formation of intervesicular saposin C dimers as a bridge between acidic phospholipid vesicles (18). This fusogenic property is thought to be involved in the maturation of multivesicular bodies (19). Dissection of the saposin C peptide and *in vitro* and *in vivo* studies indicate regional localization of these multiple functions to specific regions of the protein, including neuritogenic activity and GCase activation (20). The fusogenic and neuritogenic activities localize to the 40 amino acids of the N-terminal, whereas the COOH-half contains the GCase activation domain (20). The former functions can be duplicated with the appropriate saposin C peptide fragments. In comparison, activation of GCase requires the COOH-half within a 'saposin' structure with intact disulfide bonds. The N-terminal 35–40 amino acid sequence is not critical to this GCase activation function, as the corresponding peptide sequence from saposin B can fulfill the overall requirements (20,21).

Point mutations of human saposin C present as variants of Gaucher disease. A neuronopathic (type 3) variant phenotype was associated with a C385F mutation, whereas an apparent non-neuronopathic variant occurred in the presence of an L394P substitution (8,9,22). The neuronopathic variant showed a progressive neurological deterioration and increased GC levels in the brain (9).

To facilitate dissection of the physiological roles of saposin C, a mouse containing a knock-in of a cysteine-to-proline substitution in saposin C was created. The resultant saposin C-deficient mice presented with slowly developing neurological impairment that correlated with mild GSL accumulation and CNS pathology.

RESULTS

Generation and verification of saposin C-deficient mice

The codon for the fifth cysteine of saposin C was mutated (Cys→Pro) in the targeting vector (Fig. 1A) to destroy the disulfide bond that stabilizes the saposin C protein (4). The recombinant ES cells were screened by PCR and confirmed by Southern blot analysis (Fig. 1B). The mutation in saposin C was confirmed by DNA sequencing. To remove the *neo* gene in the targeting vector, heterozygous F1 mice were bred with ZP3-Cre transgenic mice. Subsequently, the Cre transgene was eliminated by crosses into WT C57BL6 mice (Fig. 1C). No differences in phenotype or histology were observed between saposin C−/− mice with or without the *neo* gene. Both sexes were used in the analyses, and no differences in phenotype or biochemistry were found. Mendelian ratios of saposin C−/− mice were obtained from the heterozygote crosses. Heterozygote (saposin C+/−) mice were normal phenotypically and biochemically and indistinguishable from WT. The saposin C−/− male and female mice attained the weight of WT litter mates and were fertile at maturity.

The protein levels of prosaposin and the individual saposins in saposin C−/− mice were determined by immunoblot analyses. Saposin C protein was not detected in fibroblasts (Fig. 2A) or tissues (data not shown) from saposin C−/− mice using our anti-mouse saposin C antibody. The level of prosaposin in saposin C−/− mouse fibroblasts was slightly higher than that in WT mice detected with our anti-mouse saposin D antibody (Fig. 2B). Saposin A, B and D protein in saposin C−/− liver and cultured fibroblasts were ∼50–70% of WT levels.

Phenotype and neurobehavioral assessments

Saposin C−/− mice slowly developed neurological impairment and lived up to 24 months. The onset of neurological deficits began at 10–12 months with progressive wobbling, lack of coordination, hind limb weakness and abnormal leg reflexes (Fig. 3). Ataxia developed after 12 months. No differences in phenotype were observed between males and females.

Neurobehavioral studies were conducted at 9 and 13 months in male saposin C−/− mice. On the narrow bridges test, saposin C−/− mice exhibited significant increases in latency and foot slips on round (11, 17 and 28 mm) (Fig. 4A) and square (12 and 25 mm) (data not shown) beams relative to WT mice. All saposin C−/− mice failed to cross the 5 mm square beam, whereas WT mice had no difficulty traversing the bridge (data not shown). Saposin C−/− mice showed increases in latency and number of slips with age. The elevated zero-maze tests for anxiety and fearfulness. Saposin C−/− mice spent longer times in open areas than WT control mice and concurrently had fewer open area entries (Fig. 4B), suggesting a decrease in anxiety-like behavior. Spontaneous locomotion testing measures exploratory and motor functions. Compared with age-matched WT mice, saposin C−/− mice showed greater vertical activity (rears) within the 60 min of testing, further suggesting a reduction of exploratory anxiety (Fig. 4C). Horizontal activity (total distance) was not significantly different in saposin C−/− mice from WT mice (Fig. 4C). These results indicate that deficiency of saposin C affects movement, coordination, anxiety behaviors.

Long-term potentiation (LTP) was measured in the hippocampus at 4 and 24 months Compared with WT mice, saposin C−/− mice showed significantly reduced LTP at 24 months (Fig. 5), suggesting deficiency of saposin C altered hippocampal plasticity, a cellular marker associated with learning and memory. No significant difference in LTP was observed in the mice at 4 months (data not shown).

Histopathological analyses

Saposin C−/− mice had foamy storage material in the dorsal root ganglion starting at 25 weeks. Larger axonal spheroids were evident in the dorsal horn of the spinal cord (Fig. 6A). No storage cells were visible in the brain. Pro-inflammation in saposin C−/− mice was assessed using anti-CD68 and anti-GFAP antibody staining (Fig. 6B). CD68 is an intracellular membrane glycoprotein that is expressed in quiescent and activated tissue macrophages (23). GFAP is an astrocytic marker. The enhanced GFAP signals indicate astrogliosis. Clearly enhanced CD68 and GFAP signals were found in spinal cord, brainstem,

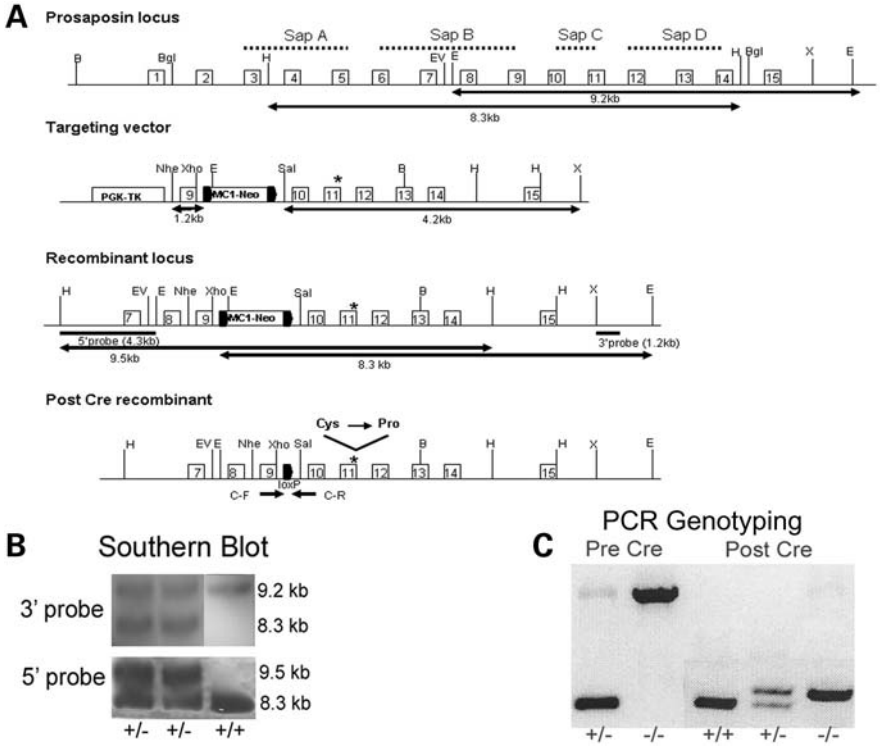

Figure 1. Targeting construct and verification. (**A**) Schematic map of the saposin C targeting construct. Individual saposins are encoded by the exons underlined with a dotted line. The mutation in the saposin C (Cys→Pro) domain was in prosaposin exon 11. The point mutation destroyed one of three disulfide bridges within saposin C, which leads to a deficiency in saposin C protein. The *neo* gene was removed by recombination of two *lox*P sites by cross-breeding of saposin C heterozygotes and Zp3-Cre transgenic mice. B, *Bam*HI; Bgl, *Bgl*II; H, *Hin*dIII; E, *Eco*RI; Ev, *Eco*RV; X, *Xba*I; Xho, *Xho*I; Nhe, *Nhe*I; Sal, *Sal*I; *mutation site. (**B**) Correct targeting of ES cells was confirmed by Southern blot. The clones were digested by *Hin*dIII for 5′ probe and *Eco*RI for 3′ probe. (**C**) PCR genotyping of saposin C mice before and after Cre recombination using primers C−F and C−R across the *lox*P site.

hindbrain, cerebellum and thalamic regions in saposin C−/− mice compared with WT mice. Disease progression was evident in H&E stained paraffin sections of spinal cord and cerebellum in 3–19-month-old saposin C−/− mice (Fig. 6C). Axonal spheroids were present in spinal cord dorsal horn after 6 months, but absent at 3 months. The Purkinje cell layer in cerebellar lobule IV was normal at 3 months. Loss of Purkinje cells was observed after 6 months. TUNEL assays of paraffin sections were negative suggesting that loss of Purkinje cells was not by an apoptotic mechanism. Visceral organs in saposin C−/− mice were not distinguishable from WT mice.

Loss of Purkinje cells in the cerebellum was evident at 2 months and progressed chronologically from lobule III to X, demonstrated by anti-calbindin antibody staining (Fig. 7A), such that by 24 months Purkinje cells were absent in lobules III to VIII. Calbindin staining revealed the degeneration of Purkinje cell axons in molecular layers and the appearance of spheroids in neuronal processes in cerebellar white matter of saposin C−/− mice (Fig. 7B). In addition, granule cell atrophy was demonstrated by decreased NeuN-stained cells in the granule cell layer (Fig. 7D). The Purkinje cell loss was subsequent to granule cell atrophy. Cerebellar reduction in C−/− was particularly evident at >20 months (Fig. 7A and C). In the same regions, increases in astrogliosis and activated microglial cells were evident (Fig. 7D).

Ultrastructural analyses revealed that axonal and neuronal processes contained electron-dense complex membrane whirl inclusions in saposin C−/− mice at 18 months (Fig. 8). The storage inclusion materials are heterogeneous and membrane bound bodies. The inclusion bodies were found in spinal cord, brainstem, midbrain, cortex, hippocampus, cerebellum and sciatic nerve. The sciatic nerve exhibited inclusion bodies and degenerating myelin layers. More neuronal processes containing inclusions were observed at 18 or 22 months than that at 10 months. No inclusions or excesses of multivesicular bodies were found in cerebral neurons or Purkinje cells at 10, 18 and 22 months (Fig. 8).

Biochemical analysis

GSLs in 13-month-old saposin C−/− mice showed increases in spinal cord GC (1.4-fold) and GS (1.3-fold) compared with WT mice (Fig. 9A and B). The LacCer levels (Fig. 9C) in the spinal cord were unchanged, but LacSph (Fig. 9D) was 2.3-fold higher than in the WT controls. In the cerebellum, the GC and GS of saposin C−/− mice were at WT levels at 13 months. Both LacCer and LacSph accumulated in the saposin C−/− mouse cerebellum to 1.9- and 1.6- fold of WT levels, respectively. No significant changes of ceramides and hydroxy ceramides were found in the cerebellum or spinal cord. The cerebral cortex, midbrain, liver and lung of saposin C−/− mice had no significant alteration of GSLs relative to the WT control.

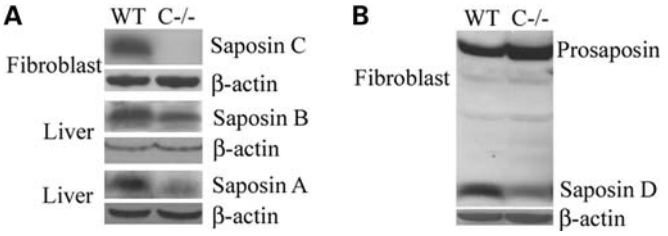

Figure 2. Saposin protein expression. (**A**) Saposin C was not detected in the fibroblasts using anti-mouse saposin C antibody. Saposin A and B were detected by anti-mouse saposin A and B antibodies, respectively. (**B**) Prosaposin and saposin D were detected with anti-mouse saposin D antibody. Prosaposin levels in saposin C−/− fibroblasts were slightly increased compared to the WT control. β-Actin was used as a loading control.

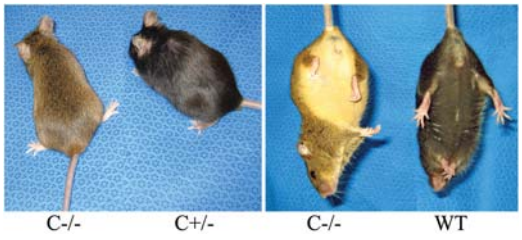

Figure 3. Phenotype of saposin C−/− mice at 16 months. (Left) Saposin C−/− mouse showing hind paw spreading suggesting paralysis. (Right) Saposin C−/− mouse with abnormal hindleg positioning and WT mouse with a normal V shape position in tail-hanging reflex.

GCase activity in tissues was assayed with 4MUG as substrate (24). In comparison to WT mice, saposin C −/− mice at 2 months showed decreases in GCase activity by ∼50% in liver, lung, spleen and brain (Fig. 10A). GCase protein levels in saposin C−/− liver were 67% of WT levels (Fig. 10B). GCase activity and protein level in heterozygote (saposin C+/−) mice were not different from that in WT mice.

DISCUSSION

To understand the functions of saposin C *in vivo*, a saposin C-deficient mouse was created in the presence of near-normal amounts of saposins A, B and D that are derived from prosaposin. The primary manifestations in the saposin C−/− mouse were of neurodegeneration that was slow in onset and slow to progress. Within the CNS, the spinal cord and cerebellum were the primary organs involved and in particular showed axonal ballooning, neuronal loss and axonal deterioration, particularly in the spinal cord. In the cerebellum, granule cell loss was followed by Purkinje cell loss that progressed from lobules III to X, with resultant decreases in cerebellar size. Within the cerebellum, astrogliosis and some infiltration by CD68+ microglial cells indicated a significant pro-inflammatory reaction. Importantly, at both the light microscopic and the ultrastructural levels, the cerebral cortical neurons and hippocampal neurons were unchanged compared with saposin C+/− littermates, yet hippocampal LTP in Schaefer collaterals was severely reduced. Biochemically, minor storage of GC and GS was present in the spinal cord, and some increases in LacCer and LacSph were present in the cerebellum, with minor changes in LacSph in the spinal cord. No histological storage was evident in visceral tissues, and the levels of GSL in the visceral tissues were normal. The deficiency of saposin C as well as the resultant histological and biochemical changes in the CNS and in the viscera, were accompanied by decreases in GCase activity and protein, thus verifying the effect of saposin C as a proteolytic protector for GCase within the lysosome (7). These findings provide insight into the functions of saposin C independent of its function in the degradation of GC, and highlight potential previously unrecognized functions related to LacSph. Because of the ultrastructural inclusions evident in axons of the saposin C−/− mice, the current findings indicate cellular effects on axonal transport and secondary retrograde neuronal degeneration. Interestingly, the previously observed increase in multivesicular body formation in prosaposin-deficient mouse models (25) was not seen in the isolated saposin C-deficient mice described here.

The data presented demonstrate that saposin C is a non-essential enhancer for GC degradation *in vivo* at the levels produced in these mice *in vivo*, i.e. GCase residual activity is present, whereas with an essential activator, a total deficiency of GCase function would exist. The total absence of GCase is incompatible with extra uterine survival in the mouse. However, saposin C optimizes the hydrolysis of GC by GCase (12), and probably also of GS. Importantly, saposin C is a stabilizer of GCase in lysosomes, protecting it from proteolytic digestion (7). When saposin C is absent in the presence of a detrimental mutation in GCase, the activity of GCase drops below a threshold level and enhances the accumulation of GC and GS in various tissues (Sun *et al*., in review). Thus, saposin C appears to be an optimizer of GCase activity: it interacts with GCase, whether mutant or WT, and protects these enzymes against proteolytic digestion by lysosomal proteases.

Although total deficiency did not lead to massive increases in GC or GS in all tissues, excluding the spinal cord, saposin C could facilitate the hydrolysis of other GSLs *in vivo*. Specifically, *in vitro* saposin C is involved in the metabolism of LacCer and ceramide (26). Also, both saposin C and B enhance the degradation of LacCer (10). The unchanged levels of LacCer in the saposin C deficient mice in the visceral tissues, cerebral cortex and spinal cord, were not unexpected since saposin B can compensate for the deficiency of saposin C. In addition, the normal levels of ceramide in the saposin C deficient mice indicate a compensatory effect of saposins D and C in the degradation of ceramide by acid ceramidase (27,28).

Of interest were the significant increases in LacCer and LacSph in the cerebellum of the saposin C deficient mice. Such accumulations, particularly of LacCer, were also found in prosaposin deficiency and in Niemann-Pick C mice (29–31). LacCer is a bioactive lipid that has been shown to participate in osteoclastogenesis, angiogenesis and neural inflammation (32–34). The biological activities of LacSph have not been well studied, but in analogy to other lysophinoglipids, GS and galactosylsphingosine, this lysolipid probably has significant toxicity to sensitive tissues, including neurons. Indeed, LacSph mobilizes calcium in isolated brain microsomes

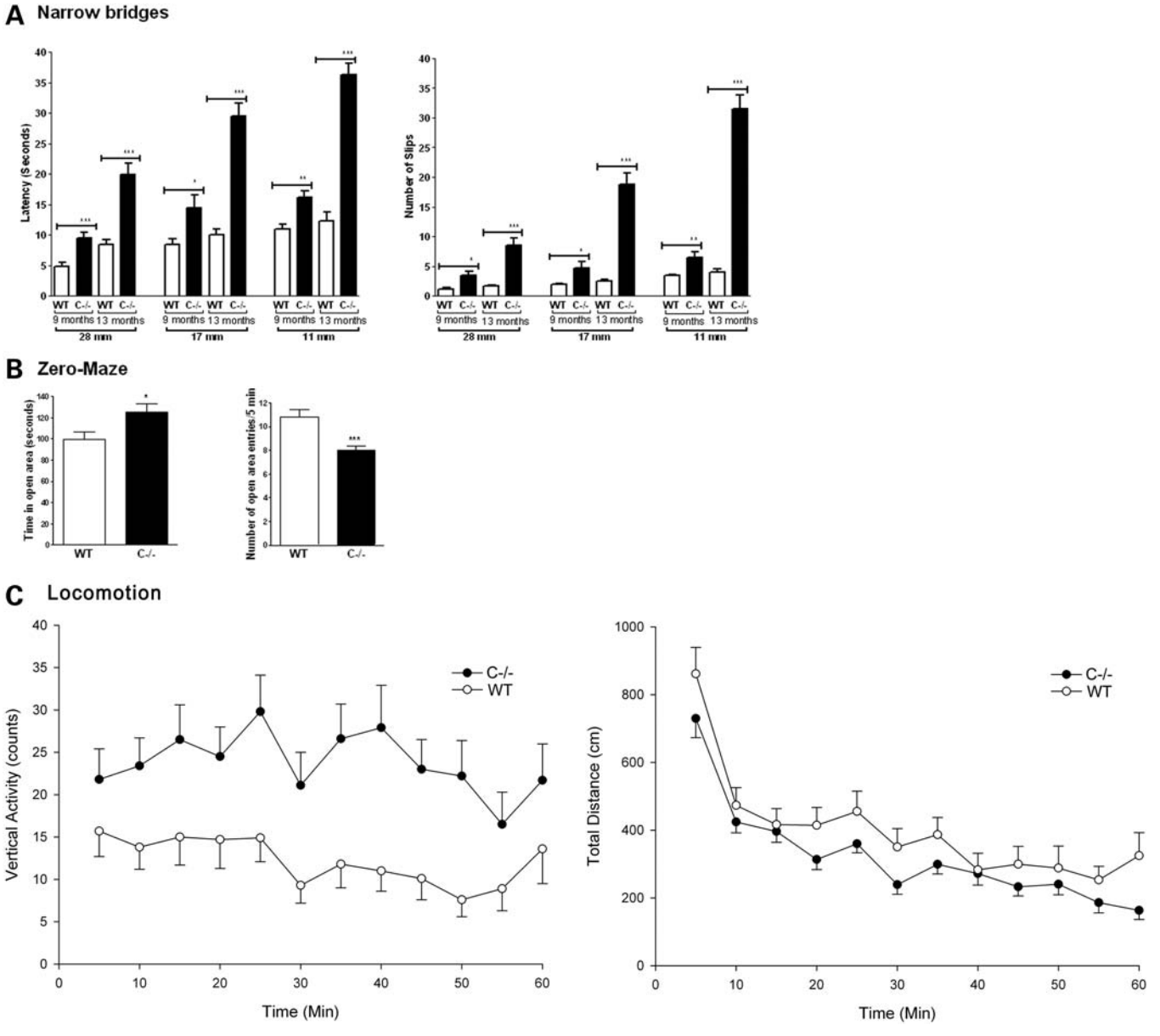

Figure 4. Neurobehavioral assessment. (**A**) Narrow bridges test. WT and saposin C−/− mice were tested on 11, 17 and 28 mm round beams at 9 and 13 months. Saposin C−/− mice showed significant increases of latency (left) across the beam and foot slips (right) compared with WT. Latency and number of slips in saposin C−/− mice progressively increased with age. (**B**) Zero-maze test. Relative to WT, saposin C−/− mice had fewer entries and spent longer time in the open area. (**C**) Locomotor activity. (Left) Saposin C−/− mice exhibited significantly enhanced vertical activity ($P < 0.02$) compared with WT. (Right) Total distance activity in saposin C−/− mice was not different from WT ($P < 0.1$). Activity was recorded every 5 min over a 60-min period. WT and saposin C−/− male mice were used in the tests. $^{*}P \leq 0.05$; $^{**}P \leq 0.01$; $^{***}P \leq 0.001$. WT, $n = 16$; saposin C−/−, $n = 21$.

(35), suggesting its participation in a pathway that could lead to neuropathological consequences and neuronal inflammation. Similar to several other lysosomal storage diseases (36,37), saposin C deficient mice showed sensitivity of Purkinje cells to the disease state. Why this should be true for Purkinje cells, and secondarily granule cells that show specific degeneration in particular lysosomal storage diseases and in the saposin C deficient mice, is unknown, but this sensitivity has now been observed in several models, including saposin D, Niemann-Pick C, Niemann-Pick A, Chediak-Higashi syndrome, neuronal ceroid lipofucinoses and lysosomal acid phosphatase (36–41), indicating vulnerability of these cells to metabolic abnormalities including GSL.

In prosaposin-deficient mice and humans, fibroblasts and other tissues have been shown to have increased numbers of multivesicular bodies (42,43). This has led to the suggestion that prosaposin and its function in GSL metabolism may be critical to the formation of multivesicular bodies, endosomes and lysosomes (42,44). However, in the CNS of the saposin C deficient mice no increase in multivesicular bodies was observed by EM studies. These studies were applied to both cortical neurons and the Purkinje cells. Consequently,

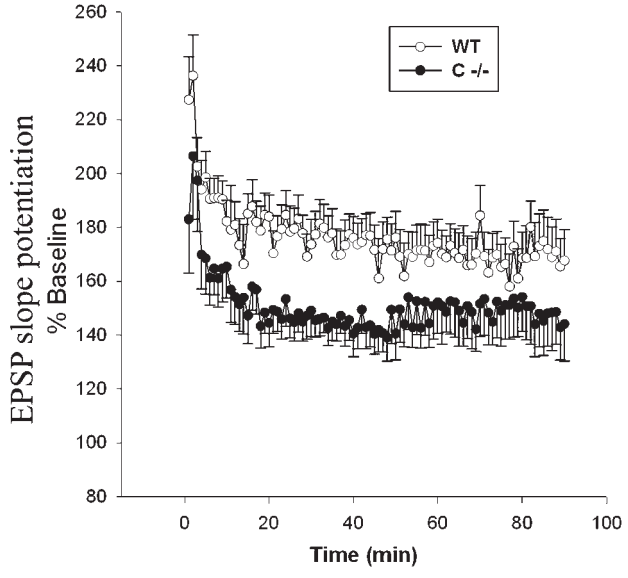

Figure 5. Electrophysiology analysis of long-term potentiation (LTP). The fEPSPs were recorded from parasagittal sections (350 μm) of hippocampal CA1 region using the MED64 multielectrode array system to determine the slope of resulting EPSPs. The slopes of the EPSPs (LTP) in 24-month-old saposin C−/− mice (closed circle) were significantly ($P < 0.05$) decreased compared with WT mice (open circle) for 90 min following stimulation. WT, $n = 7$ mice; saposin C−/−, $n = 6$ mice.

multivesicular bodies formation does not appear to be a mechanism involved in pathologic degeneration in the cortex, cerebellum or spinal cord. Cell death caused by apoptosis was unlikely in these mice as suggested by negative TUNEL assay. However, saposin C may have additional functions in cellular metabolism beyond that for the degradation of GSLs, particularly GC, GS, LacCer and LacSph. As is evident in the spinal cord, retrograde axonal degeneration was present as evidenced by the large deposits in the dorsal horn of the spinal cord. This correlated with the presence of inclusion bodies within the axons and suggests a mechanism of retrograde degeneration caused by saposin C deficiency. The precise role in this transport process and potential release at synapses remains to be elucidated, but it seems to be fundamental to the pathological processes within the CNS.

The clinical and pathological phenotype presented in saposin C−/− mice was primarily related to neuronal dysfunction. Massive Purkinje cell death occurred in cerebellum. The spheroids that contained inclusion bodies were found in axons. These pathological defects correlated with the phenotype of ataxia and decreased coordination in saposin C−/− mice. Axonal spheroids have been noted in several lysosomal storage diseases, including Niemann-Pick C, GM2 gangliosidoses, α-*N*-acetylgalactosaminidase and α-mannosidosis (45–48). Early findings on these lysosomal disease animal models suggest that the loss of Purkinje cells is secondary to axonal dystrophy (48). The axonal dystrophy may affect anterograde or retrograde transport, which can cause axonal degeneration and cell death, as suggested in Alzheimer's disease and other neurodegenerative disorders (49,50). Deterioration of neuromotor function and impaired hippocampal LTP could be the result of such axonal dysfunction. Saposin C is a lysosomal protein, and lysosomes in the neuron are located in the soma. Further studies will be required to define how the deficiency of saposin C leads to axonal spheroids.

MATERIALS AND METHODS

Materials

Reagents from commercial sources: anti-fade/DAPI, methyl green, ABC Vectastain and alkaline phosphatase kit II (Black) (Vector Laboratory, Burlingame, CA), DIG Easy Hyb, anti-digoxigenin-AP, CDP-Star, positively charged nylon membranes and Lumi-film chemiluminescent detection film (Roche Applied Science, Indianapolis, IN), Qiagen Quick-change II XL kit (Qiagen, Inc., Valencia, CA), restriction enzymes (New England Labs, Beverly, MA), NuPAGE 4–12% Bis–Tris gel, NuPAGE MES SDS running buffer, AlexaFluor488 goat anti-mouse IgG (H+L) (Invitrogen, Carlsbad, CA), 4-methylumbelliferyl-β-D-glucopyranoside (4MUG, Sigma), M-PER Mammalian Protein Extraction Reagent and BCA protein assay reagent (Pierce, Rockford, IL) and Hybond^{TM}–ECL^{TM} nitrocellulose membrane and ECL detection reagent (Amersham Biosciences, Piscataway, NJ).

Construction of targeting vector and generation of saposin C−/− mice

Saposin C-deficient mice were created by knocking in a codon change to create the substitution cysteine-to-proline (C→P) substitution in saposin C. This mutation eliminates one of this protein's three disulfide bridges and results in a selective deficiency in this saposin. The same strategy has been used previously (4,28,38,51). The mouse prosaposin genomic DNA clones and targeting vector (OSdupdel) were kindly provided by Dr Kunihiko Suzuki. The knock-in saposin C was created using a Qiagen Quick-change II XL kit with mismatched oligonucleotide primers: C5F (5′-AGC TCT CTG CCC GGG GTG ATC GGC CTC TG-3′), C5R (5′-CA GAG GCC GAT CAC CCC GGG CAG AGA GCT-3′). The mismatched nucleotides are underlined. The short arm of the 1.2 kb *Nhe* I–*Xho* I fragment was generated by PCR using a pBluescript subclone 7–9 containing exons 8–15 of the mouse prosaposin gene as a template. The resultant product was cloned into the TopoTA (PCR II) vector. Using the same subclone 7-9, the long arm of 4.2 kb *Sal* I–*Xba* I fragments encoding Cys→Pro was generated by PCR and cloned into the *Sal* I/*Xba* I sites of the TA cloning vector. The OSdupdel vector contains polymer enhancer/herpes simplex virus thymidine kinase (MC1) promoter with the neomycin (*neo*) gene flanked by two *lox*P sites and the thymidine kinase (TK) gene driven by the 3′ phosphoglycerate kinase (*PGK*) promoter (30). The long arm (4.2 kb) carrying the requisite mutation was ligated into *Sal*I/*Xba*I sites downstream of MC1-*neo* and formed the 3′ homologous region. The short arm (1.2 kb) was cloned into *Nhe*I/*Xho*I sites upstream of MC1-*neo* in the vector and formed the 5′ homologous region. The sequences of long arm and short arm were confirmed by direct sequencing. The targeting vector was linearized by *Not*1 and introduced into a 129/SvEv ES cell line.

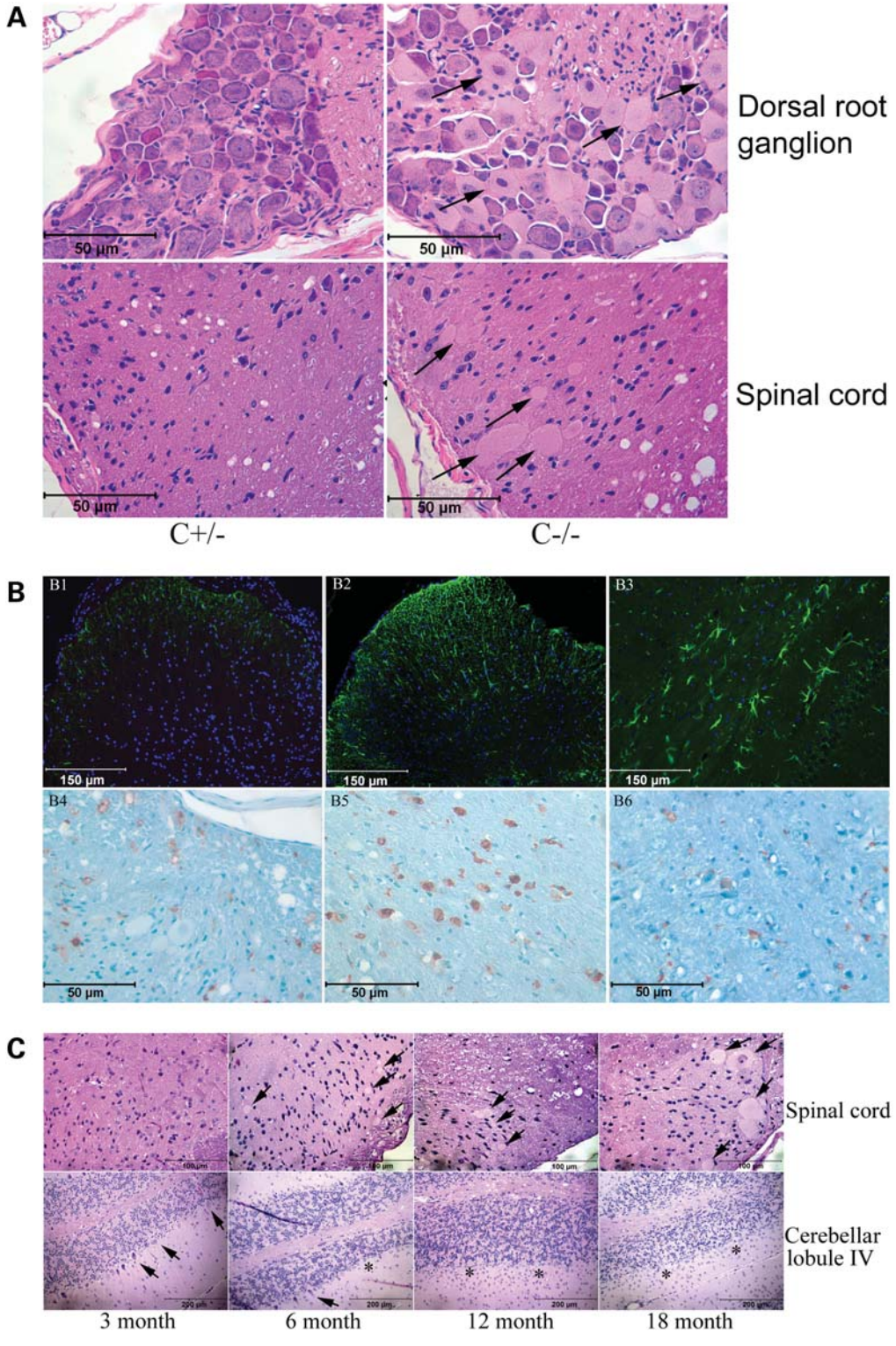

Figure 6. CNS pathology in C−/− mice. (**A**) The paraffin sections of dorsal root ganglion and dorsal horn of spinal cord from 15-month-old saposin C+/− or C−/− mice were stained with H&E. Foamy storage material (arrows) was present in the dorsal root ganglion neurons of saposin C−/− mice. Larger axonal spheroids (arrows) were present in the spinal cord dorsal horn of these mice. As a control, saposin C+/− mice had normal morphology in dorsal root ganglion and spinal cord. (**B**) CNS proinflammation in saposin C−/− mice demonstrated by anti-GFAP (B1-B3) and anti-CD68 (B4-B6). (**B1**) WT spinal cord, (**B2**) saposin C−/− spinal cord and (**B3**) C−/− midbrain at 15 months showed astrogliosis with enhanced GFAP (green) signal. The nucleus was labeled by DAPI (blue). (B4) C−/− dorsal horn of spinal cord. (B5) C−/− thalamus. (B6) C−/− brain stem. Microglial cells were stained by anti-CD68 antibody (brown) in 24-month-old saposin C−/− mice. Tissue sections were counterstained with hematoxylin. (**C**) H&E stained paraffin sections of spinal cord and cerebellum from saposin C−/− mice at 3, 6, 12 and 18 months. Axonal spheroids were present in dorsal horn of spinal cord at 6, 12 and 18 months, but absent at 3 months. Purkinje cell layer (arrows) in cerebella lobule IV was normal at 3 months. Loss of Purkinje cells (*) was evident at 6 months and older.

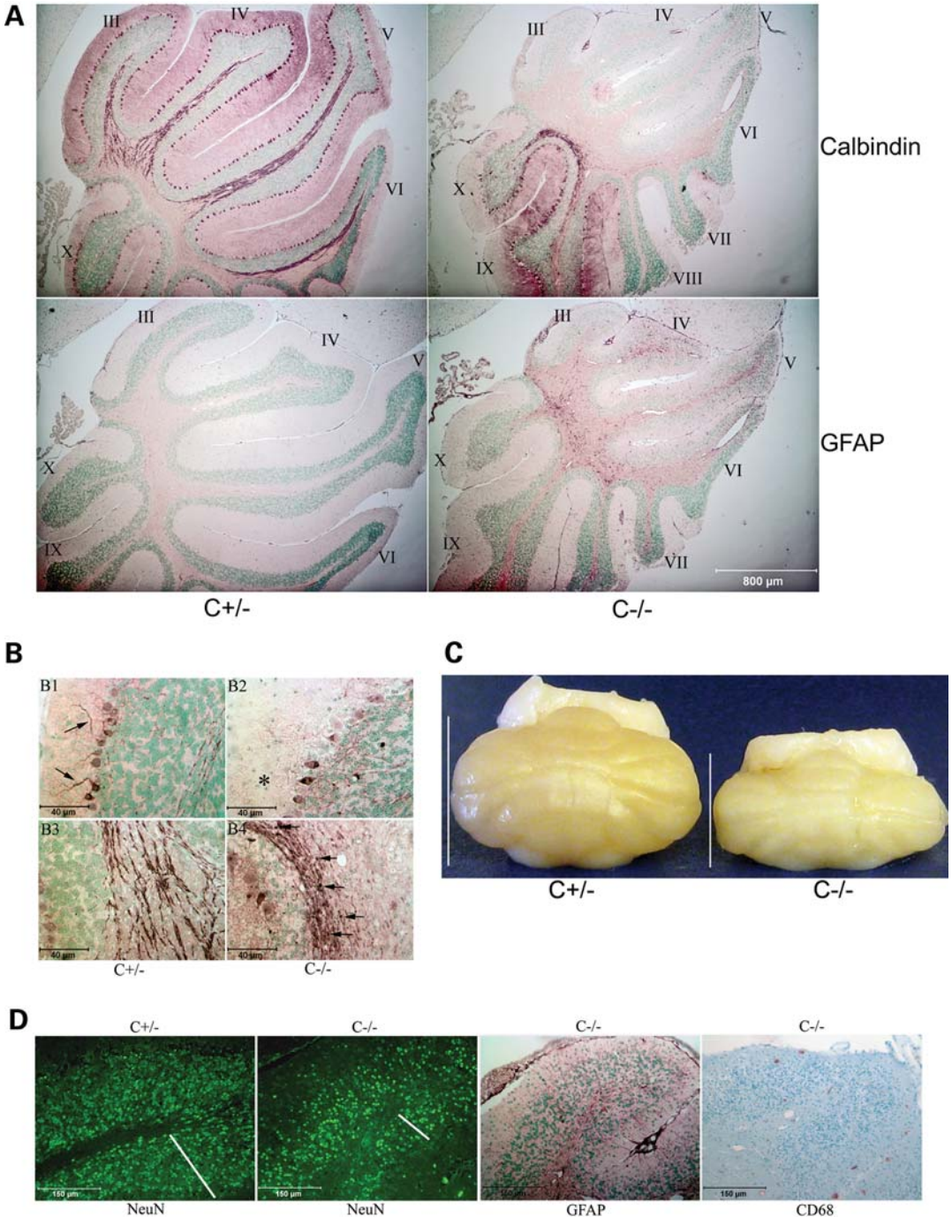

Figure 7. Pathology in cerebellum. (**A**) Anti-calbindin antibody stained Purkinje cells (brown) in 24-month-old C+/− and C−/− mouse brain. Loss of Purkinje cells in saposin C−/− mice progressed from cerebella lobule III to X with age. Increases of astrogliosis demonstrated by anti-GFAP antibody staining (brown) were in the region where the Purkinje cells were lost. Normal Purkinje cell layers and astrocytes were found in the C+/− cerebellum. (**B**) Calbindin staining revealed axon and neuronal processes in the molecular layer and white matter of the cerebellum. (**B1**) Normal Purkinje cells and axons (arrows) in C+/− mouse. (**B2**) Degeneration of Purkinje cell axons (stars) in the molecular layer of cerebella lobule X in 24-month-old C−/− mouse. (**B3**) Neuronal processes in C+/− cerebella white matter. (**B4**) Neural spheroids (arrows) presented in the neuronal processes of C−/− mouse. (**C**) 24-month-old C+/− and C−/− mouse cerebellum. The white bars show the height of cerebellum. The size of saposin C−/− cerebellum was reduced at 24 months. (**D**) Atrophy in the granule cell layer of saposin C−/− mice. NeuN staining cells (green) were decreased in the granulecell layer of cerebella lobule III from 24-month-old C−/− mice compared with lobule III of C+/− mouse. The white bar in the photo shows the diameter of the granule cell layer. Both GFAP (brown) and CD68 (brown) signals were enhanced in lobule III of the saposin C−/− mouse. Sections stained with calbindin and GFAP were counterstained with methyl green (green). CD68-stained sections were counterstained with hemotoxilin.

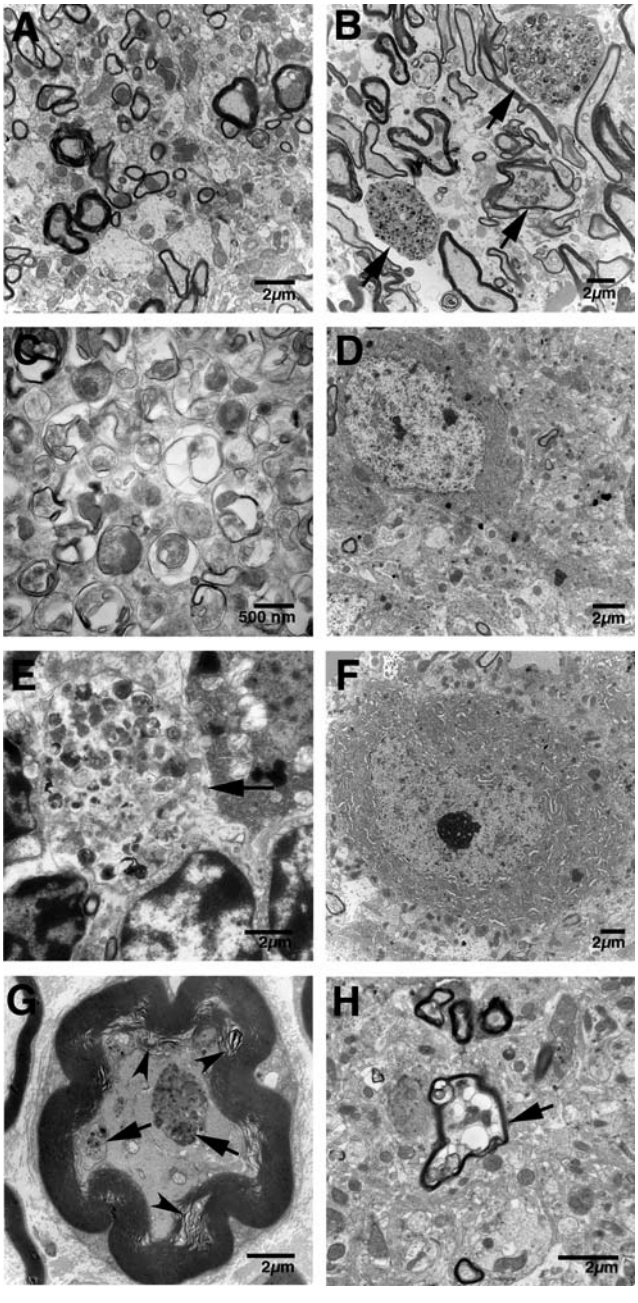

Figure 8. Ultrastructural studies. (**A**) The spinal cord of saposin C+/− mice at 18 months had normal morphology. (**B**) The spinal cord of saposin C−/− mice at 18 months showed inclusion bodies (arrows) in neuronal process. (**C**) Enlarged view of inclusion bodies in (B). (**D**) Cortical neuron in saposin C−/− mice at 10 months had normal morphology. (**E**) Axonal inclusions (arrow) in granule cell layer of saposin C−/− cerebellum at 18 months. (**F**) Purkinje cells in saposin C−/− mouse at 10 months had normal morphology. (**G**) The sciatic nerve of saposin C−/− mice at 18 months had inclusion materials (arrows) and degenerating myelin layers (arrowheads). (**H**) Axonal inclusion material (arrow) in the midbrain of saposin C−/− mice at 18 months.

PCR analysis was conducted to screen the recombinant ES clones using the primers flanking outside of the short arm: C-ES F1-25 (5′-GGTAGCATTGCATGTCTTAGCGCTG-3′) and inside of the short arm: C-ES F5 (5′-GAGTGGGTCTG TTCTGAACATTGCTT-3′), in combination with the primer in the 5′ region of *neo*, NEO2R (5′-AAC CAC ACT GCT CGA CAT TGG GTG-3′). The recombinant clones generated 1.6 kb and the wild-type (WT) clones had 1.4 kb PCR products, respectively. The recombinant ES clones were further confirmed by Southern blot analysis. Identified recombinant ES cells were amplified and DNA (10 μg) from each clone was digested with *Hin*dIII or *Eco*RI. Southern blots were probed with DIG labeled 5′ or 3′ probes (28). In the recombinant ES clones, *Hin*dIII digestion generated 8.3 kb WT and 9.5 kb recombinant fragments, identified by 5′-probe and *Eco*RI digestion, and resulted in 9.2 kb WT and 8.3 kb recombinant fragments with the 3′-probe. The mutations in the recombinant clones were verified by PCR and sequencing. Correctly targeted clones were used to generate chimeric mice by microinjection into C57BL/6J blastocysts. Electroporation, ES cell culture, selection and chimera breeding were carried out by the Gene-Targeting Mouse Service Core at the University of Cincinnati. To remove the *neo* gene, the heterozygous F1 mice were crossed into Zp3-Cre mice (C57BL/6-TgN(Zp3-Cre)93Knw purchased from The Jackson Laboratory) (52) as described (28). The strain of background for saposin C−/− is C57BL/6J/129SvEV. All mice were maintained in micro-isolators, with the exception of those going through behavior, in accordance with institutional guidelines under IACUC approval at Cincinnati Children's Research Foundation.

PCR genotyping

PCR reaction was conducted for routine mouse colony genotyping using the genomic DNA from clipped tails. After validation by sequencing of the mutations within saposin C, the *lox*P site was used as a marker for the point mutation genotyping with the primers C loxP F (5′-CAGATACCCCATCC TCCCATGG-3′) and C loxP R (5′-TGTGAAGGACAAG AGGAGAGTG-3′). The PCR product of WT was 200 bp, mutant with *neo* was 1.4 kb and without *neo* was 307 bp.

Histological studies

Following CO_2 narcosis, mice were perfused with saline and then 4% paraformaldehyde. The tissues were dissected and fixed in 10% formalin, embedded in paraffin, sectioned and stained with hemotoxilin and eosin (H&E). Paraffin sections of cerebellum were stained with mouse anti-calbindin D28K (Sigma, C9848) and mouse anti-GFAP (Sigma, G3893). The antibodies were diluted 1/500 or 1/200 in PBS with 3% goat serum and 0.2% Triton X-100, respectively. Detection was with ABC Vectastain and the alkaline phosphatase kit II (Black), according to the manufacturer's instructions. The slides were counterstained with methyl green. For immunofluorescence staining, frozen sections from 4% paraformaldhyde fixed tissues were incubated with mouse anti-GFAP (1/200). Paraffin sections were reacted with mouse anti-NeuN (1/100) (Chemicon, MAB377). The antibodies were diluted in PBS with 3% normal goat serum and 0.2% Triton X-100. Both biotinylated goat anti-mouse and streptavidin-conjugated fluorescent 480 (green) were applied to the sections. The samples were counterstained with antifade/DAPI. The signals were visualized with a Zeiss Axiovert 200M microscope equipped with an Apotome. CD68 monoclonal antibody (Serotec, FA-11) staining

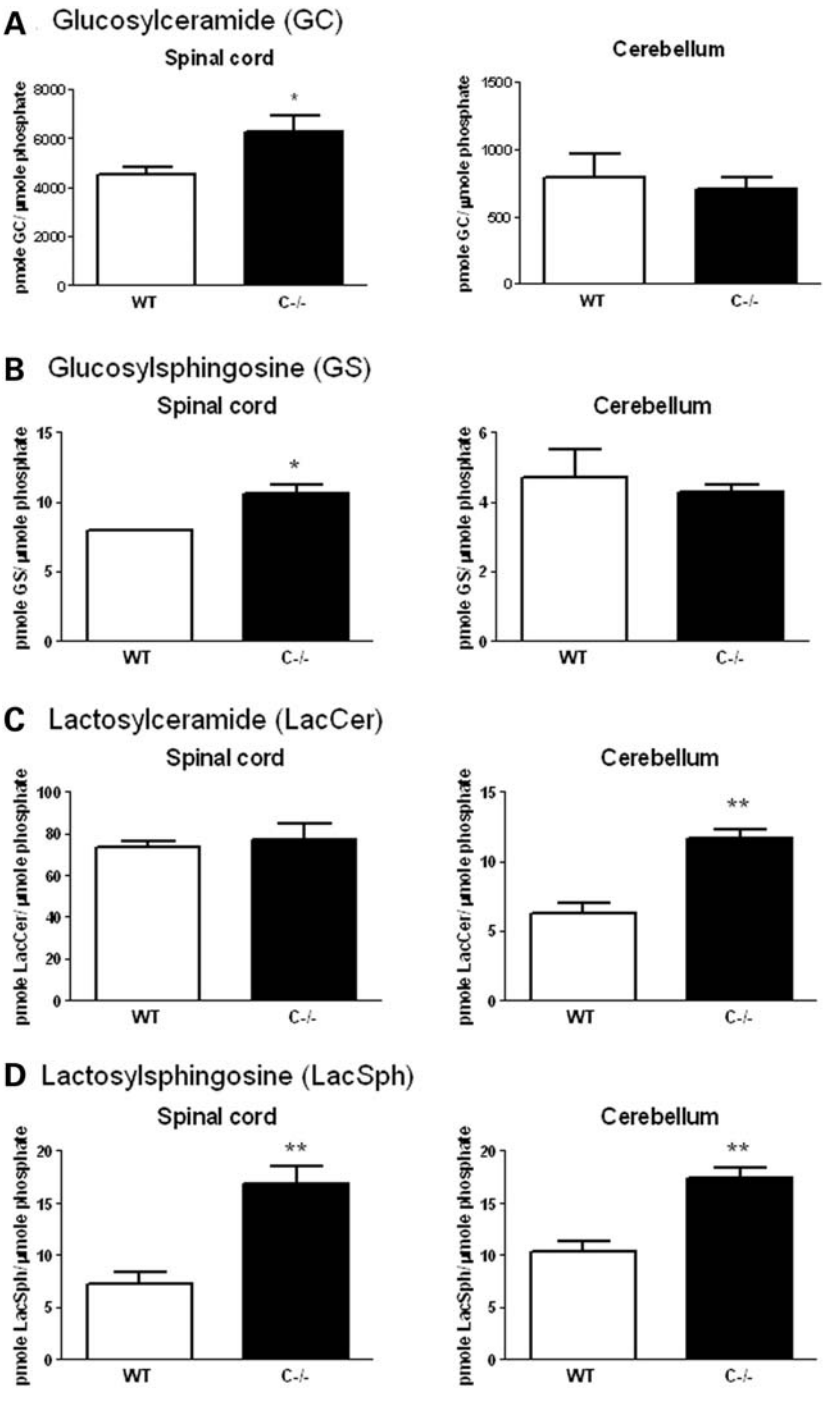

Figure 9. GSL analyses. Spinal cord and cerebellum lysate were analyzed for GC, GS, LacCer and LacSph. Saposin C−/− mice had significant increases of GC, GS and LacSph in the spinal cord. LacCer and LacSph increased in the C−/− cerebellum. The amounts of lipids were normalized to phosphate in each sample. Age-matched 13-month-old WT and C−/− mice were used in the assay ($n = 3$). $^{*}P \leq 0.05$ and $^{**}P \leq 0.01$.

on the frozen sections was as described (53). Karnovsky's fixative was used for ultrastructural studies.

Immunoblot

Tissues or cell extracts (50–200 μg) were prepared in M-PER (Mammalian Protein Extraction Reagent) and separated on NuPAGE 4–12% Bis–Tris gel with NuPAGE MES SDS running buffer, and electro-blotted on Hybond^{TM}–ECL^{TM} nitrocellulose membranes. The membranes were blocked in 3% BSA for 1 h, followed by incubation overnight with the rabbit anti-mouse saposin D, C, A or B antibodies (1/500 in 0.15% milk and 1% BSA) to detect individual saposins and prosaposin (28). Mouse anti β-actin monoclonal antibody (1/10 000 in 2% w/v dry milk) was applied to detect β-actin. The signal was developed using ECL detection reagent

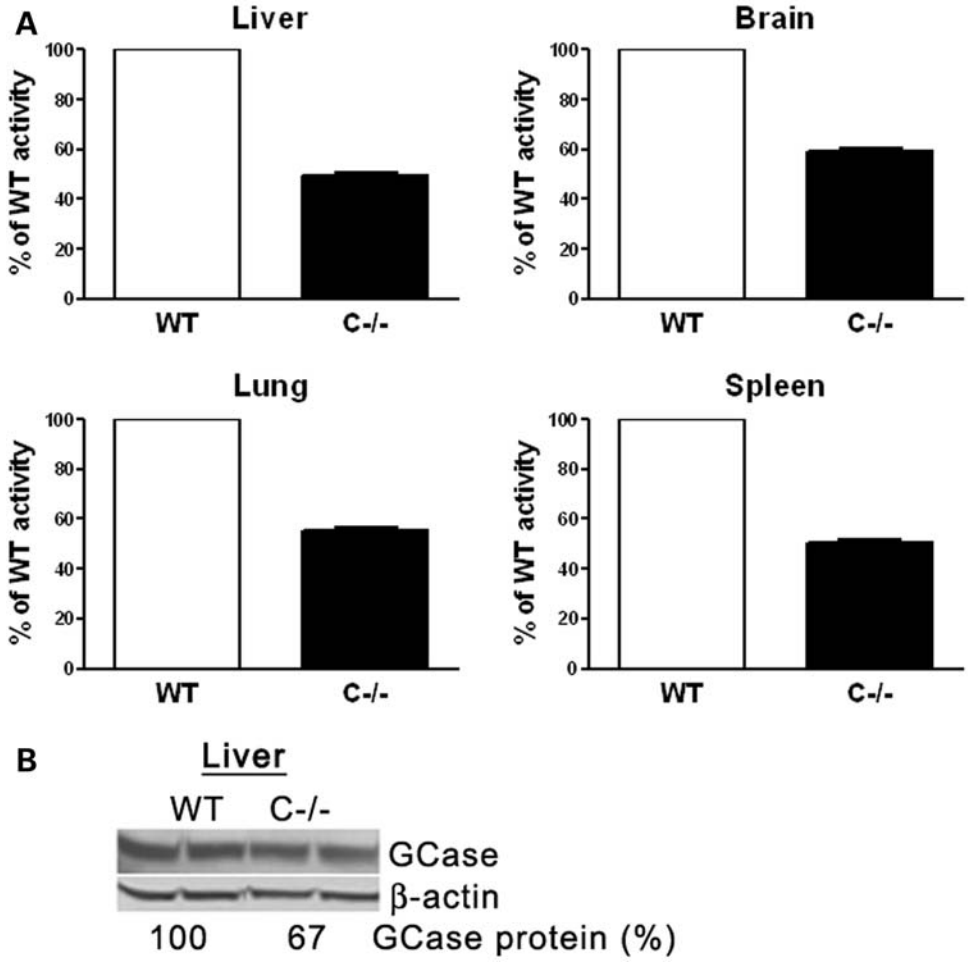

Figure 10. GCase activity and protein in C−/− mice. (**A**) GCase activity levels were decreased in C−/− liver, lung, brain and spleen by ∼50% relative to the WT level. (**B**) The GCase protein level in the C−/− liver was 67% of the WT level. Age-matched 2-month-old WT and C−/− mice were used in the assay ($n = 3$).

according to the manufacturer's instructions. Protein concentration was determined using BCA protein assay reagent.

GCase activity and protein

Mouse GCase activity assay (54) and protein detection was described previously (55). The amounts of GCase proteins were quantitated by ImageQuant software relative to the amount of β-actin in the same sample.

Tissue GSL analyses

Monohexosylceramides (GC and galactosylceramide), LacCer, GS, lactosylsphingosine (LacSph) and ceramide were quantified by LC/MS in the Lipidomic Core at the Medical University of South Carolina (56). Because C−/− mice had normal levels of saposin A and galactosylceramidase, C−/− and WT mice should have the same levels of galactosylceramide. Consequently, the alterations of monohexosylceramide in the analyses reflect changes in GC. The GSL contents were normalized to phosphate content in the same sample after lipid extraction from tissue lysate. Three animals from each genotype were included in the analyses. Data were analyzed by Student's *t*-test using GraphPad Prism 5.0 software.

Behavioral studies

The behavioral tests were conducted in the Animal Behavioral Collaborative Core at Cincinnati Children's Research Foundation.

Narrow bridges. Square beams (1 m) 25, 12 and 5 mm wide and round beams (1 m) with diameters of 28, 17 and 11 mm were used as described (57). The mice were trained by traversing the 12 mm beam for three consecutive days, four trials per day. Animals were considered to be trained when they crossed the 12 mm beam in <20 s. The test phase began on the fourth day. Each mouse in turn received two consecutive trials (up to 60 s/trial) on each square or round beam in a progression from widest to narrowest. Latency to traverse each beam and the number of times the hind foot slipped off the beam were recorded. A total of 26 saposin C−/− mice at 13 months and 17 WT male mice were tested as sex (male) and age-matched groups. Data were analyzed by Student's *t*-test using GraphPad Prism 5.0 software.

Tail-hanging reflex observations. Mice were lifted by the tail to observe the leg reflexes every month. The legs of normal mice assume a V position, whereas the affected mice with advanced disease exhibited an abnormal position of the legs and clasped paws. The age at first development of this abnormality was recorded.

Elevated zero-maze test. The apparatus was ring-shaped, and behavior was recorded with an overhead camera connected to a DVD-R. The circular runway was 105 cm in diameter with a 10 cm path width. Two quadrants of the ring were enclosed by black acrylic sidewalls and two quadrants were open; the latter had a 1 cm clear acrylic curb to prevent slipping off the edge. Overhead lights were turned off; a single dim halogen light source was used. Mice were placed in the enclosed quadrant and tested for 5 min. Test sessions were recorded and scored later for time in open area, head dip frequency and number of open area entries. A total of 26 saposin C−/− male mice at 13 months and 17 age-matched WT male mice were tested. Data were analyzed by Student's *t*-test using GraphPad Prism 5.0 software.

Locomotor activity. Locomotor activity was measured in a 41 × 41 × 30 cm Accuscan activity monitor equipped with 16 pairs of photodetector-LED beams along the *x* and *y* axes (Accuscan Electronics with VersaMax software, Columbus, OH). The test was conducted under normal overhead fluorescent light. Individual mice were placed in the chambers for 60 min. The apparatus was cleaned with 70% ethanol between animals. Total horizontal distance and vertical activity (rears) were recorded in 5-min intervals. Saposin C−/− ($n = 26$) and WT ($n = 17$) male mice were tested at 13 months. Data were analyzed with a mixed model 2-way analysis of variance (Proc GLM, SAS, SAS Institute, Cary, NC) with interval as the repeated measure.

Electrophysiology

Electrophysiology was performed using the MED64 multi-electrode array system (Alpha Med Sciences) as described (4). Parasagittal sections (350 μm) were taken from the hippocampus of male WT ($n = 7$) and C−/− mice ($n = 6$) at 24 months. Stimulation and recording of resulting fEPSPs were from the Schaffer collateral pathway of the CA1 region of the hippocampus. Slopes of EPSPs following high-frequency stimulation were recorded for 90 min. Brain slices were recorded in duplicate for each animal and the data were averaged per animal. Data were recorded using Performer 2.0 software (Alpha Med Sciences). Data were analyzed using repeated measures ANOVA with gene as a between subject factor and time as a within subject factor, the repeated measure were the fEPSP measurements following LTP induction.

ACKNOWLEDGEMENTS

The authors thank Benjamin Liou, Venette Inskeep, Brian Quinn and Juying Xu for their technical assistance; Lisa McMillin, Meredith Farmer, Sabina Sylvest, Georgianne Ciraolo and Chris Woods for skilled tissue preparation and photomicrographs; and Brandy Morris for her clerical expertise.

Conflict of Interest statement. None declared.

FUNDING

We thank the Lipidomics Core, supported in part by NIH C06 PR018823, at the Medical University of South Carolina. Electrophysiology study was supported by a grant to M.T.W. (R01 ES 015689). This work was supported by grants to G.A.G (R01 NS/DK 36681).

REFERENCES

1. Leonova, T., Qi, X., Bencosme, A., Ponce, E., Sun, Y. and Grabowski, G.A. (1996) Proteolytic processing patterns of prosaposin in insect and mammalian cells. *J. Biol. Chem.*, **271**, 17312–17320.
2. Sandhoff, K., Kolter, T. and Van Echten-Deckert, G. (1998) Sphingolipid metabolism. Sphingoid analogs, sphingolipid activator proteins, and the pathology of the cell. *Ann. NY Acad. Sci.*, **845**, 139–151.
3. Li, S.C., Sonnino, S., Tettamanti, G. and Li, Y.T. (1988) Characterization of a nonspecific activator protein for the enzymatic hydrolysis of glycolipids. *J. Biol. Chem.*, **263**, 6588–6591.
4. Sun, Y., Witte, D.P., Ran, H., Zamzow, M., Barnes, S., Cheng, H., Han, X., Williams, M.T., Skelton, M.R., Vorhees, C.V. *et al.* (2008) Neurological deficits and glycosphingolipid accumulation in saposin B deficient mice. *Hum. Mol. Genet.*, **17**, 2345–2356.
5. Zhang, X.L., Rafi, M.A., DeGala, G. and Wenger, D.A. (1990) Insertion in the mRNA of a metachromatic leukodystrophy patient with sphingolipid activator protein-1 deficiency. *Proc. Natl Acad. Sci. USA*, **87**, 1426–1430.
6. Qi, X. and Grabowski, G.A. (1998) Acid beta-glucosidase: intrinsic fluorescence and conformational changes induced by phospholipids and saposin C. *Biochemistry*, **37**, 11544–11554.
7. Sun, Y., Qi, X. and Grabowski, G.A. (2003) Saposin C is required for normal resistance of acid beta-glucosidase to proteolytic degradation. *J. Biol. Chem.*, **278**, 31918–31923.
8. Rafi, M.A., de Gala, G., Zhang, X.L. and Wenger, D.A. (1993) Mutational analysis in a patient with a variant form of Gaucher disease caused by SAP-2 deficiency. *Somat. Cell Mol. Genet.*, **19**, 1–7.
9. Pampols, T., Pineda, M., Giros, M.L., Ferrer, I., Cusi, V., Chabas, A., Sanmarti, F.X., Vanier, M.T. and Christomanou, H. (1999) Neuronopathic juvenile glucosylceramidosis due to sap-C deficiency: clinical course, neuropathology and brain lipid composition in this Gaucher disease variant. *Acta. Neuropathol (Berl).*, **97**, 91–97.
10. Zschoche, A., Furst, W., Schwarzmann, G. and Sanhoff, K. (1994) Hydrolysis of lactosylceramide by human galactosylceramidase and GM1-beta-galactosidase in a detergent-free system and its stimulation by sphingolipid activator proteins, sap-B and sap-C. Activator proteins stimulate lactosylceramide hydrolysis. *Eur. J. Biochem.*, **222**, 83–90.
11. Qi, X. and Grabowski, G.A. (2001) Molecular and cell biology of acid beta-glucosidase and prosaposin. *Prog. Nucleic. Acid. Res. Mol. Biol.*, **66**, 203–239.
12. Qi, X., Leonova, T. and Grabowski, G.A. (1994) Functional human saposins expressed in Escherichia coli. Evidence for binding and activation properties of saposins C with acid beta-glucosidase. *J. Biol. Chem.*, **269**, 16746–16753.
13. Harzer, K., Paton, B.C., Christomanou, H., Chatelut, M., Levade, T., Hiraiwa, M. and O'Brien, J.S. (1997) Saposins (sap) A and C activate the degradation of galactosylceramide in living cells. *FEBS Lett.*, **417**, 270–274.
14. Azuma, N., O'Brien, J.S., Moser, H.W. and Kishimoto, Y. (1994) Stimulation of acid ceramidase activity by saposin D. *Arch. Biochem. Biophys.*, **311**, 354–357.
15. Vaccaro, A.M., Salvioli, R., Barca, A., Tatti, M., Ciaffoni, F., Maras, B., Siciliano, R., Zappacosta, F., Amoresano, A. and Pucci, P. (1995) Structural analysis of saposin C and B. Complete localization of disulfide bridges. *J. Biol. Chem.*, **270**, 9953–9960.

16. Alattia, J.R., Shaw, J.E., Yip, C.M. and Prive, G.G. (2007) Molecular imaging of membrane interfaces reveals mode of beta-glucosidase activation by saposin C. *Proc. Natl Acad. Sci. USA*, **104**, 17394–17399.
17. You, H.X., Qi, X. and Yu, L. (2004) Direct AFM observation of saposin C-induced membrane domains in lipid bilayers: from simple to complex lipid mixtures. *Chem. Phys. Lipids*, **132**, 15–22.
18. John, M., Wendeler, M., Heller, M., Sandhoff, K. and Kessler, H. (2006) Characterization of human saposins by NMR spectroscopy. *Biochemistry*, **45**, 5206–5216.
19. Wang, Y., Grabowski, G.A. and Qi, X. (2003) Phospholipid vesicle fusion induced by saposin C. *Arch. Biochem. Biophys.*, **415**, 43–53.
20. Qi, X., Qin, W., Sun, Y., Kondoh, K. and Grabowski, G.A. (1996) Functional organization of saposin C. Definition of the neurotrophic and acid beta-glucosidase activation regions. *J. Biol. Chem.*, **271**, 6874–6880.
21. Qi, X., Kondoh, K., Yin, H., Wang, M., Ponce, E., Sun, Y. and Grabowski, G.A. (2002) Ex vivo localization of the mouse saposin C activation region for acid beta-glucosidase. *Mol. Genet. Metab.*, **76**, 189–200.
22. Tylki-Szymanska, A., Czartoryska, B., Vanier, M.T., Poorthuis, B.J., Groener, J.A., Lugowska, A., Millat, G., Vaccaro, A.M. and Jurkiewicz, E. (2007) Non-neuronopathic Gaucher disease due to saposin C deficiency. *Clin. Genet.*, **72**, 538–542.
23. Gordon, S., Lawson, L., Rabinowitz, S., Crocker, P.R., Morris, L. and Perry, V.H. (1992) Antigen markers of macrophage differentiation in murine tissues. *Curr. Top. Microbiol. Immunol.*, **181**, 1–37.
24. Xu, Y.H., Ponce, E., Sun, Y., Leonova, T., Bove, K., Witte, D. and Grabowski, G.A. (1996) Turnover and distribution of intravenously administered mannose-terminated human acid beta-glucosidase in murine and human tissues. *Pediatr. Res.*, **39**, 313–322.
25. Chu, Z., Sun, Y., Kuan, C.Y., Grabowski, G.A. and Qi, X. (2005) Saposin C: neuronal effect and CNS delivery by liposomes. *Ann. NY Acad. Sci.*, **1053**, 237–246.
26. Kolter, T. and Sandhoff, K. (2005) Principles of lysosomal membrane digestion: stimulation of sphingolipid degradation by sphingolipid activator proteins and anionic lysosomal lipids. *Annu. Rev. Cell Dev. Biol.*, **21**, 81–103.
27. Klein, A., Henseler, M., Klein, C., Suzuki, K., Harzer, K. and Sandhoff, K. (1994) Sphingolipid activator protein D (sap-D) stimulates the lysosomal degradation of ceramide in vivo. *Biochem. Biophys. Res. Commun.*, **200**, 1440–1448.
28. Sun, Y., Witte, D.P., Zamzow, M., Ran, H., Quinn, B., Matsuda, J. and Grabowski, G.A. (2007) Combined saposin C and D deficiencies in mice lead to a neuronopathic phenotype, glucosylceramide and alpha-hydroxy ceramide accumulation, and altered prosaposin trafficking. *Hum. Mol. Genet.*, **16**, 957–971.
29. Hulkova, H., Cervenkova, M., Ledvinova, J., Tochackova, M., Hrebicek, M., Poupetova, H., Befekadu, A., Berna, L., Paton, B.C., Harzer, K. *et al.* (2001) A novel mutation in the coding region of the prosaposin gene leads to a complete deficiency of prosaposin and saposins, and is associated with a complex sphingolipidosis dominated by lactosylceramide accumulation. *Hum. Mol. Genet.*, **10**, 927–940.
30. Fujita, N., Suzuki, K., Vanier, M.T., Popko, B., Maeda, N., Klein, A., Henseler, M., Sandhoff, K. and Nakayasu, H. (1996) Targeted disruption of the mouse sphingolipid activator protein gene: a complex phenotype, including severe leukodystrophy and wide-spread storage of multiple sphingolipids. *Hum. Mol. Genet.*, **5**, 711–725.
31. Walkley, S.U. and Suzuki, K. (2004) Consequences of NPC1 and NPC2 loss of function in mammalian neurons. *Biochim. Biophys. Acta.*, **1685**, 48–62.
32. Fukumoto, S., Iwamoto, T., Sakai, E., Yuasa, K., Fukumoto, E., Yamada, A., Hasegawa, T., Nonaka, K. and Kato, Y. (2006) Current topics in pharmacological research on bone metabolism: osteoclast differentiation regulated by glycosphingolipids. *J. Pharmacol. Sci.*, **100**, 195–200.
33. Rajesh, M., Kolmakova, A. and Chatterjee, S. (2005) Novel role of lactosylceramide in vascular endothelial growth factor-mediated angiogenesis in human endothelial cells. *Circ. Res.*, **97**, 796–804.
34. Won, J.S., Singh, A.K. and Singh, I. (2007) Lactosylceramide: a lipid second messenger in neuroinflammatory disease. *J. Neurochem.*, **103** (Suppl. 1), 180–191.
35. Lloyd-Evans, E., Pelled, D., Riebeling, C. and Futerman, A.H. (2003) Lyso-glycosphingolipids mobilize calcium from brain microsomes via multiple mechanisms. *Biochem. J.*, **375**, 561–565.
36. Ko, D.C., Milenkovic, L., Beier, S.M., Manuel, H., Buchanan, J. and Scott, M.P. (2005) Cell-autonomous death of cerebellar purkinje neurons with autophagy in Niemann-Pick type C disease. *PLoS Genet.*, **1**, 81–95.
37. Sleat, D.E., Wiseman, J.A., El-Banna, M., Kim, K.H., Mao, Q., Price, S., Macauley, S.L., Sidman, R.L., Shen, M.M., Zhao, Q. *et al.* (2004) A mouse model of classical late-infantile neuronal ceroid lipofuscinosis based on targeted disruption of the CLN2 gene results in a loss of tripeptidyl-peptidase I activity and progressive neurodegeneration. *J. Neurosci.*, **24**, 9117–9126.
38. Matsuda, J., Kido, M., Tadano-Aritomi, K., Ishizuka, I., Tominaga, K., Toida, K., Takeda, E., Suzuki, K. and Kuroda, Y. (2004) Mutation in saposin D domain of sphingolipid activator protein gene causes urinary system defects and cerebellar Purkinje cell degeneration with accumulation of hydroxy fatty acid-containing ceramide in mouse. *Hum. Mol. Genet.*, **13**, 2709–2723.
39. Rudelius, M., Osanger, A., Kohlmann, S., Augustin, M., Piontek, G., Heinzmann, U., Jennen, G., Russ, A., Matiasek, K., Stumm, G. *et al.* (2006) A missense mutation in the WD40 domain of murine Lyst is linked to severe progressive Purkinje cell degeneration. *Acta. Neuropathol.*, **112**, 267–276.
40. Mannan, A.U., Roussa, E., Kraus, C., Rickmann, M., Maenner, J., Nayernia, K., Krieglstein, K., Reis, A. and Engel, W. (2004) Mutation in the gene encoding lysosomal acid phosphatase (Acp2) causes cerebellum and skin malformation in mouse. *Neurogenetics*, **5**, 229–238.
41. Macauley, S.L., Sidman, R.L., Schuchman, E.H., Taksir, T. and Stewart, G.R. (2008) Neuropathology of the acid sphingomyelinase knockout mouse model of Niemann-Pick A disease including structure-function studies associated with cerebellar Purkinje cell degeneration. *Exp. Neurol.*, **214**, 181–192.
42. Chu, Z., Witte, D.P. and Qi, X. (2005) Saposin C-LBPA interaction in late-endosomes/lysosomes. *Exp. Cell Res.*, **303**, 300–307.
43. Harzer, K., Paton, B.C., Poulos, A., Kustermann-Kuhn, B., Roggendorf, W., Grisar, T. and Popp, M. (1989) Sphingolipid activator protein deficiency in a 16-week-old atypical Gaucher disease patient and his fetal sibling: biochemical signs of combined sphingolipidoses. *Eur. J. Pediatr.*, **149**, 31–39.
44. Morales, C.R., Fuska, J., Zhao, Q. and Lefrancois, S. (2001) Biogenesis of lysosomes in marshall cells and in cells of the male reproductive system. *Mol. Reprod. Dev.*, **59**, 54–66.
45. Wolfe, D.E., Schindler, D. and Desnick, R.J. (1995) Neuroaxonal dystrophy in infantile alpha-N-acetylgalactosaminidase deficiency. *J. Neurol. Sci.*, **132**, 44–56.
46. Ohara, S., Ukita, Y., Ninomiya, H. and Ohno, K. (2004) Axonal dystrophy of dorsal root ganglion sensory neurons in a mouse model of Niemann-Pick disease type C. *Exp. Neurol.*, **187**, 289–298.
47. Huxtable, C.R. and Dorling, P.R. (1985) Mannoside storage and axonal dystrophy in sensory neurones of swainsonine-treated rats: morphogenesis of lesions. *Acta. Neuropathol.*, **68**, 65–73.
48. Walkley, S.U., Baker, H.J., Rattazzi, M.C., Haskins, M.E. and Wu, J.Y. (1991) Neuroaxonal dystrophy in neuronal storage disorders: evidence for major GABAergic neuron involvement. *J. Neurol. Sci.*, **104**, 1–8.
49. Grutzendler, J., Helmin, K., Tsai, J. and Gan, W.B. (2007) Various dendritic abnormalities are associated with fibrillar amyloid deposits in Alzheimer's disease. *Ann. NY Acad. Sci.*, **1097**, 30–39.
50. Coleman, M. (2005) Axon degeneration mechanisms: commonality amid diversity. *Nat. Rev. Neurosci.*, **6**, 889–898.
51. Matsuda, J., Vanier, M.T., Saito, Y., Tohyama, J. and Suzuki, K. (2001) A mutation in the saposin A domain of the sphingolipid activator protein (prosaposin) gene results in a late-onset, chronic form of globoid cell leukodystrophy in the mouse. *Hum. Mol. Genet.*, **10**, 1191–1199.
52. Lewandoski, M., Wassarman, K.M. and Martin, G.R. (1997) Zp3-cre, a transgenic mouse line for the activation or inactivation of loxP-flanked target genes specifically in the female germ line. *Curr. Biol.*, **7**, 148–151.
53. Sun, Y., Quinn, B., Witte, D.P. and Grabowski, G.A. (2005) Gaucher disease mouse models: point mutations at the acid beta-glucosidase locus combined with low-level prosaposin expression lead to disease variants. *J. Lipid. Res.*, **46**, 2102–2113.
54. Xu, Y.H., Quinn, B., Witte, D. and Grabowski, G.A. (2003) Viable mouse models of acid beta-glucosidase deficiency: the defect in Gaucher disease. *Am. J. Pathol.*, **163**, 2093–2101.

55. Sun, Y., Quinn, B., Witte, D.P. and Grabowski, G.A. (2005) Gaucher disease mouse models: point mutations at the acid {beta}-glucosidase locus combined with low-level prosaposin expression lead to disease variants. *J. Lipid. Res.*, **46**, 2102–2113.
56. Bielawski, J., Szulc, Z.M., Hannun, Y.A. and Bielawska, A. (2006) Simultaneous quantitative analysis of bioactive sphingolipids by high-performance liquid chromatography-tandem mass spectrometry. *Methods*, **39**, 82–91.
57. Sun, Y., Jia, L., Williams, M.T., Zamzow, M., Ran, H., Quinn, B., Aronow, B.J., Vorhees, C.V., Witte, D.P. and Grabowski, G.A. (2008) Temporal gene expression profiling reveals CEBPD as a candidate regulator of brain disease in prosaposin deficient mice. *BMC Neurosci.*, **9**, 76.